A Kinetic and Morphological Study of Barite Precipitation Reaction in the Presence of Fe^{3+} and Mn^{2+} Ions

Lassaad Mechi
Department of Chemistry, College of Science, University of Ha'il, Ha'il, Saudi Arabia | Laboratory of Materials and Environment for Sustainable Development, Tunis El Manar University, Tunisia
mechilassaad@yahoo.fr

Received: 16 April 2024 | Revised: 4 May 2024 | Accepted: 10 May 2024

 DOI: https://doi.org/10.48084/etasr.7518

ABSTRACT

The precipitation mode of barium sulphate ($BaSO_4$) in the presence of mineral additives plays an important role in many industrial processes. Therefore, in this paper, a study of the precipitation reaction of a saturated barium sulphate solution in the presence of metal ions Fe^{3+} and Mn^{2+}, found in industrial waters and in the geochemical evolutions of paleoenvironments, is presented. XRD, conductivity, FTIR spectroscopy, and SEM were used to investigate the barite precipitation reaction in the presence of a known amount of Fe^{3+} and Mn^{2+} ions. Conductivity measurements showed that the presence of Fe^{3+} accelerated both induction and crystal growth stages. On the other hand, adding Mn^{2+} ions did not affect the kinetics of the precipitation reaction. Solid analysis showed that the barite lattice was doped with low levels of manganese.

Keywords-$BaSO_4$; precipitation; kinetics; structure; morphology; iron (III); Mn (II)

I. INTRODUCTION

The variation of physic-chemical parameters in a system, such as internal pressure, temperature, and pH during the extraction of petroleum and the addition of surface water with a different composition in the second recovery, can trigger tartar formation reaction. These facilitate the emergence of deposits of minerals in the well, reservoir, and machinery that transports production fluids. The geological level (blockage of the rock formation's pores) as well as the hydraulic, mechanical, thermal, and economic levels are all greatly impacted by the creation of these deposits [1]. Barite precipitation occurs outside and inside reservoirs and pipe lines. Nucleation and precipitation processes can happen on surface facilities, pumps, wells, pipelines, and in refinery equipment used for crude oil processing [2-4]. The most frequent tartars are calcium carbonate, calcium sulfate, and barium sulfate [5, 6]. The first disruptor of petroleum infrastructure and equipment is barite due to its low solubility value ($Ks_{(BaSO4)}= 1.10 \times 10^{-10}$). The literature shows that the composition of groundwater is rich in several metal ions. Furthermore, the precipitation process and the composition of the produced scale can be altered by the presence of trace amounts of metal ions. This has an impact on all efforts to prevent tartar from forming as well as the assessment of potential damage.

The impact of the metallic ions on the precipitation phenomena has been thoroughly examined with regard to the barium sulphate precipitation reaction. The final product generally has a particular percentage of metallic ions [7-9]. Several studies have examined the impact of Fe^{2+}, Eu^{2+}, Sr^{2+}, Ca^{2+}, Cs^{2+}, and Mn^{2+} ions on barite precipitation, looking at the solid state obtained outside at the end of the reaction compared to pure barite precipitation phenomena [9-12].

The effect of Fe^{3+} and Mn^{2+} on the barite precipitation reaction and the nature of the formed solid was examined in this paper.

II. EXPERIMENTAL SECTION

A. Materials

The experimental unit was designed to take out the experimental portion (Figure 1). The reaction was kept at a steady temperature of 308 K, using a thermostatic closed cell and thermostatic water circulation. To maintain homogeneity in the solution, we employed a magnetic stirrer. We were able to determine the pH and conductivity properties of the solution by using the Proline B 210 pH-meTER and the Proline B 250 conductivity cell.

B. Chemical Reagents

Barium chloride dehydrate ($BaCl_2 \cdot 2H_2O$), sodium sulphate (Na_2SO_4), iron (III) chloride ($FeCl_3$), manganese chloride ($MnCl_2$), and sodium chloride (NaCl) were used for an analytical grade supplied by SIGMA-ALDRICH and FLUKA (Belgium).

C. Experimental Procedure

To carry out the experimental part we followed the following procedure. A mixed supersaturated solution of barite

was prepared by mixing 500 mL of ($BaCl_2$, $MnCl_2$)·or ($BaCl_2$, $FeCl_3$) with 500 mL of Na_2SO_4 solution at T = 308 K (Table I). In the mixture, the initial concentration of the different reagents is equal to 5.10^{-3} M. The manipulation was performed at a starting pH= 6.2 (with pH=2.8 at the end of the reaction) for sulphate solutions in a semi-open reactor. The effect of atmospheric CO_2 on the pH and equilibrium of the solution is negligible. The literature shows that only at high pH values the precipitation reaction is affected [5]. To eliminate the effect of ionic strength on the kinetics of the reaction, the ionic strength was adjusted with the addition of NaCl. The reaction was initiated when sodium sulfate was added to the cationic solution (Ba^{2+}, Fe^{3+}, and Mn^{2+}). We analyzed the precipitate that was left behind after the reaction using FTIR, XRD, and SEM techniques. By aggregating 40 scans on an Affinity-1C Schimadzu spectrophotometer, defusing reflectance allowed for the acquisition of the infrared spectra of the samples in KBr pellets in the 4000–400 cm^{-1} region with a resolution of 4 cm^{-1}. XRD was performed at room temperature with a Jobin Yvonet: LabRam HR, utilizing Cu Kα radiation (λ = 0.15418 nm) and a Philips X'PERTPRO diffractometer in step scanning mode. The scanning range for the XRD patterns was 2 theta = 5–90°. A fixed counting period of 4 s and a short angular step of 2 h = 0.017° were applied. The software X-Pert High¬Score Plus was utilized to ascertain the identification phase and the XRD reflection positions. To guarantee the accuracy of the experiment, we replicated all precipitation reactions multiple times.

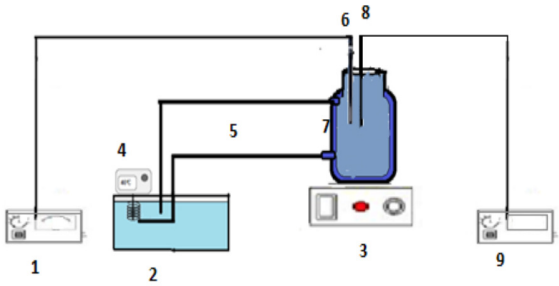

Fig. 1. Experimental unit: 1. Conductivity cell using Proline B 250; 2. Thermostatic bath; 3. Magnetic stirrer; 4. Heating head; 5. Pipes; 6. Electrode conductivity; 7. Double-wall reactor of 1000 ml; 8. Electrode pH; 9. pH meter.

III. RESULTS AND DISCUSSION

The influence of iron (III) and manganese (II) on the precipitation process of barium sulphate was examined in this work by a combination of spectroscopic, morphological, and conductivity analyses. In order to investigate the precipitation phenomenon, we prepared three synthetic solutions (Table I).

TABLE I. COMPOSITION OF SYNTHETIC SOLUTIONS FOR THE STUDY OF Fe^{3+} AND Mn^{2+} EFFECT ON BARITE PRECIPITATION

Solution	$[Ba^{2+}]$ (M)	$[SO_4^{2-}]$ (M)	$[Fe^{3+}]$ (M)	$[Mn^{2+}]$ (M)
S0	$2.5.10^{-3}$	$2.5.10^{-3}$	0	0
S1	$2.5.10^{-3}$	$2.5.10^{-3}$	$2.5.10^{-3}$	0
S2	$2.5.10^{-3}$	$2.5.10^{-3}$	0	$2.5.10^{-3}$

We decided to examine the variation in conductivity for every trial in order to have a point of comparison between the acquired results. The delta conductivity presented in Figure 2, is the variance between the conductivity at the moment t and the initial conductivity, calculated by: $\Delta\sigma = \sigma(t) - \sigma(initial)$.

A. *Effect of Fe^{3+}*

1) *Effect of Fe^{3+} Ions on Conductivity Variation*

Based on the conductivity readings taken during the reaction, Figure 2 depicts the investigation of iron (III)'s impact on the barite precipitation reaction's kinetics. The kinetics of the precipitation of barium sulphate reaction are impacted by the presence of iron (III) ion, as can be shown by comparing the variation of the conductivity in solutions S0 and S1 depicted in Figure 2. Every variation has two different parts. The first half shows a linear increase in Δσ with increasing time. This stage is related to the phases of both induction and crystal growth stages [13]. The equilibrium between the ionic species in the solution and the solid is achieved in the second step, when the value of Δσ stays constant [14]. The addition of Fe^{3+} (2.5×10^{-3} M) to the barium sulphate saturated solution (S1) caused an increase in the linear part-slope, an increase in Δσ, and a reduction in the induction and crystalline development times from 64 s to 20 s. This result is different than the what acquired after the addition of iron ions in supersaturated solution of calcium carbonate. This difference is attributed to the fact that, at low pH, the $BaSO_4$ precipitation reaction does not depend to pH as the $CaCO_3$ reaction. Additionally, the hydrolysis of water by the free Fe^{3+} ions decreases the pH of the solution from 6.2 to 2.8 [15]. Therefore, solid iron sulfate or iron oxide species may be able to accelerate the heterogeneous precipitation on the one hand and on the other hand to make a film which will reduce the homogeneous precipitation [16]. We measured the ultimate total concentration of Fe^{3+} in the barium sulfate solution at the end of the experience in order to confirm the above theory. It was discovered to be $2.4\ 10^{-3}$ M. The rusty color of the solid produced can be explained by the fact that an amount of the Fe^{3+} ions was precipitated with barium sulfate. According to [15], dissolved species that can bind to and be adsorbed by heterogeneous precipitation, such as metal cations, anions, and neutral polymer molecules, prefer to react on the surface of oxide particles scattered in water. To understand more about the impact of Fe^{3+} on the barite precipitation reaction in our case, FTIR analysis of the solid collected after filtration of the solution was carried out.

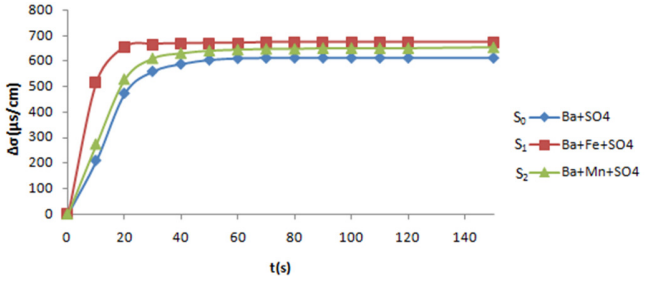

Fig. 2. Curve of the conductivity variation in barite supersaturated solution for S0, S1, and S2 at. T=308 K.

2) FTIR Spectrum Analysis

The functional groups involved in the adsorption or absorption of iron compounds generated on the crystal surface or in the barite lattice were identified using the FTIR spectra of the precipitates collected at the conclusion of the precipitation reaction of S1 solution. Any differences, indicated by the appearance of additional peaks or shifts in the strength of already existing peaks, are compared to the spectrum of pure barite. The pertinent FTIR spectra are shown in Figure 3. Peaks in the spectrum regions of 3423 and 1636 cm^{-1} indicate the existence of water in the pure barium sulphate spectrum. Furthermore, barite is identified by the sulfur-oxygen (S-O) stretching, which places the three bands of sulphate ion oscillation at 1070, 1114, and 1197 cm^{-1}. The antisymmetric banding modes of SO_4^{2-} are also responsible for the two peaks in the spectra that are depicted at 636 and 609 cm^{-1} [4, 17] Figure 3 illustrates the appearance of new peaks in the 400-840 cm^{-1} range, indicating the development of iron oxides. With a minor divergence, the FTIR spectra of hematite exhibit the usual peaks of Fe-O bonds at 461, 512, and 644 cm^{-1} [18]. Authors in [19, 20] reported the occurrence of α-FeO(OH) in relation to other peaks that were observed at 751 and 839 cm^{-1}. Peaks at 3285 and 3180 cm^{-1} are associated with the α-FeO(OH) O-H band. With a small deviation, the sulfate peaks may be seen in 606, 644, 983, 1071, 1109, and 1212 cm^{-1}. The infrared spectroscopy result shown in Figure 3 indicates that the precipitate obtained contains iron oxides and barite without any mixed solids.

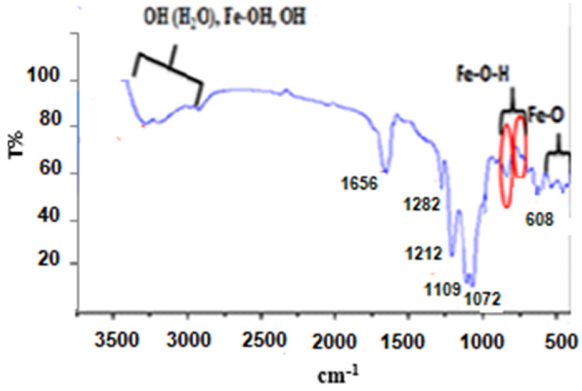

Fig. 3. FTIR spectra of $BaSO_4$:Fe^{3+} sample obtained at room temperature.

3) SEM Analysis Results

To evaluate the impact of Fe^{3+} addition on crystal shape, SEM images were gathered for later visual examination (Figure 3). Figure 3 shows the presence of pure barite with other iron solid phases.

B. Effect of Mn^{2+}

1) Effect of Mn^{2+} Ions on Crystal Growth Rate

Based on conductivity data for the liquid state and combined by morphology and structural analysis for the solid state, the influence of Mn^{2+} ions on barium sulfate deposition is shown in Figure 2. The conductivity curve in the presence of Mn^{2+} ions is identical to those of pure barite. Therefore, Mn^{2+} ions cannot significantly affect the barite precipitation kinetics. In the presence of Mn ions, there is no precipitation reaction between Mn and sulfate ions (higher solubility of $MnSO_4$ in water, solubility = 530 g in 1 kg of water). So, no important modification in heterogonous and homogenous precipitation mode of barite occurred. In addition, the solid generated by the filtration of the S2 solution was examined by XRD, SEM, and FTIR analyses in order to study the impact of Mn^{2+} ions on the resulting solid phase.

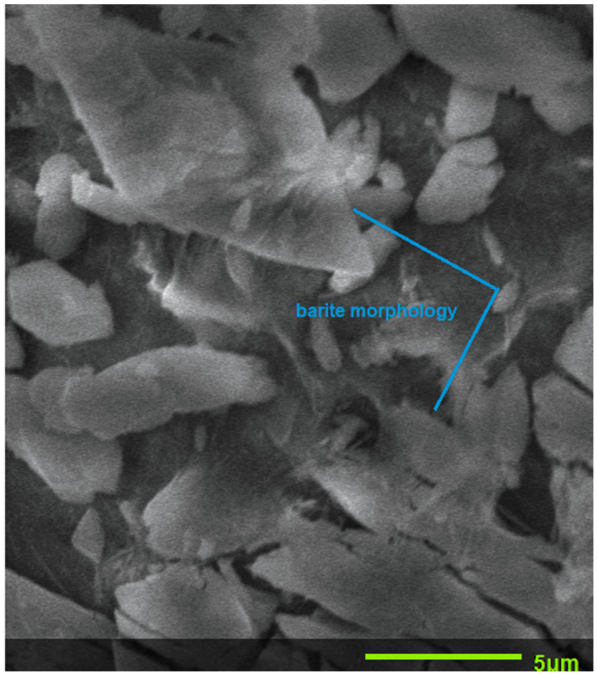

Fig. 4. SEM image of $BaSO_4$:Fe^{3+} solid sample obtained at room temperature.

2) FTIR Sectrum Analysis

There are significant variations in the S2's spectrum compared to pure barium sulphate, as demonstrated by the infrared spectra of Figure 5. There were two shifts observed in the band: one at 642 cm^{-1} (636 in pure barite), which corresponded to the SO_4's out-of-plane bending vibration, and another at 605 cm^{-1} (609 in pure barite). Furthermore, a significant deviation was noted in the 1000–1200 cm^{-1} region, which was ascribed to sulfate ion vibration in accordance with sulfur–oxygen (S–O) stretching. However, the compound's spectrum obtained in the presence of Mn^{2+} exhibits a significant shift in the peak from 1213 cm^{-1} in pure barite to 1197 cm^{-1} in S2, a shoulder between 1050 cm^{-1} and 1130 cm^{-1} and a peak at 982 cm^{-1} in pure barite shift to 979 cm^{-1}. We found also a new peak at 1383 cm^{-1}.

This leads us to conclude that the obtained result differs somewhat from pure solid barite. Authors in [5, 21, 22] showed similar variation in the infrared and Raman spectrum when they studied the role of Ca, Mn, and Sr in barite deposition. Therefore, the change in IR spectra that was observed cannot be explained by surface adsorption, but can be explained by the insertion of Mn^{2+} or the replacement of Ba^{+2} with Mn^{+2} in the

barite lattice to create a solid solution $Ba_{1-x}Mn_xSO_4$ [5, 21]. The substitution theory is ruled out by the large discrepancy from the radius of Mn^{2+} with that of Ba^{2+}. Thus, we employed the XRD and SEM investigation to validate this insertion hypothesis.

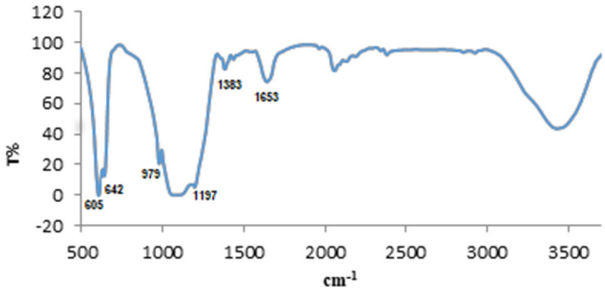

Fig. 5. FTIR spectra of $BaSO_4:Mn^{2+}$ sample obtained at room temperature.

3) XRD Analysis Results

The single-phase compound formation was examined by the XRD pattern seen in Figure 6. The strength of the peaks is the only difference of the two XRD patterns. The position (2θ) shows no difference. According to [5], the Mn/$BaSO_4$ pattern is part of the orthorhombic space group. According to [21], the weak incorporation of Mn into the $BaSO_4$ lattice is the cause of the intensity difference. The relatively high solubility of $MnSO_4$ in a water-based solution explains this result. Consequently, there is very little impact of the ion-pair amount of $MnSO_4$ to $BaSO_4$ nucleation compared to calcium effect [5].

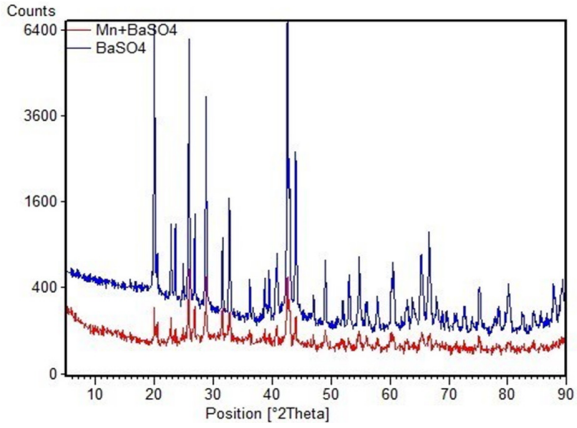

Fig. 6. XRD pattern of $BaSO_4:Mn^{2+}$ sample obtained at room temperature.

The XRD and infrared spectra match those published in[18] when $BaSO_4$ was enriched with a stoichiometric ratio of Mn^{2+} (The Mn-doped $BaSO_4$ was made by recrystallization method by mixing $BaCO_3$ and concentrated H_2SO_4 in stoichiometric ratio. The mixture of solid was heated at 650–700 ˚C in a quartz crucible for 30 min) however, we employed a different synthesis process and a stoichiometric amount of Mn^{2+}.

4) SEM Analysis Results

To evaluate the impact of Mn^{2+} inclusion on crystal shape, SEM images were gathered (Figure 7). According to [23], the barite precipitate has hexagonal platelets as its distinctive shape when Mn^{2+} is not present. The SEM image displays the shape of flattened diamonds with some morphological alterations caused by the addition of Mn^{2+} (the particles have regular hexagon-like angular edges).

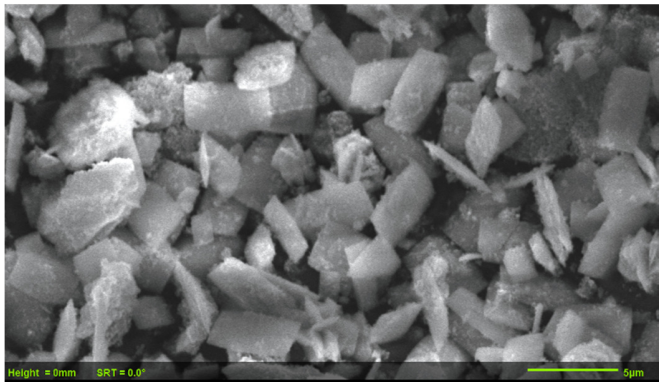

Fig. 7. SEM image of $BaSO_4:Mn^{2+}$ solid sample obtained at room temperature.

We can infer from the examination of the compounds derived from solution S2 that the existence of Mn^{2+} cannot modify the kinetics, due to the absence of any modification in heterogeneous and homogenous precipitation mode. Solid analyses can confirm slight doping of the barite lattice.

IV. CONCLUSION

This work examined the effect of adding metal cations, such as manganese (II) and iron (III) ions, on the formation of barium sulfate through the precipitation reaction. This study showed the formation of iron precipitate, without changing in the barite structure. The conductivity study demonstrated that the addition of iron Fe^{3+} increases the global rate of the precipitation reaction. Indeed, the induction time decreased and the slope of the conductivity curve increased at the start of the reaction. This can be attributed to the acceleration of the heterogeneous mode. During this reaction, an important variation of the pH attributed to $Fe(OH)_3$ formation was noticed. On the other hand, this investigation demonstrated that the presence of manganese (II) ions did not modify the precipitation kinetics of barite. FTIR, XRD, and SEM analyses confirmed a slight doping of manganese ions in barite lattice.

REFERENCES

[1] O. Hussein, C. Utton, M. Ojovan, and H. Kinoshita, "The effects of BaSO4 loading on OPC cementing system for encapsulation of BaSO4 scale from oil and gas industry," *Journal of Hazardous Materials*, vol. 261, pp. 11–20, 2013, https://doi.org/10.1016/j.jhazmat.2013.06.048.

[2] A. Ur-Rehman and Y. S. Usmani, "Field Engineers' Scheduling at Oil Rigs: a Case Study", *Engineering, Technology & Applied Science Research*, vol. 2, no. 1, pp. 155-161, Feb. 2012, https://doi.org/10.48084/etasr.95.

[3] H. Q. Vu, V. H. Tran, P. T. Nguyen, N. T. H. Le, and M. T. Le, "Radiation Shielding Properties Prediction of Barite used as Small Aggregate in Mortar," *Engineering, Technology & Applied Science Research*, vol. 10, no. 6, pp. 6469–6475, Dec. 2020, https://doi.org/10.48084/etasr.3880.

[4] R. M. S. Wat, K. S. Sorbie, A. C. Todd, P. Chen, and P. Jiang, "Kinetics of BaSO4 Crystal Growth and Effect in Formation Damage," in *SPE*

Formation Damage Control Symposium, Lafayette, LA, USA, Feb. 1992, Art. no. SPE-23814-MS, https://doi.org/10.2118/23814-MS.

[5] H. Azaza, A. Doggaz, L. Mechi, V. Optasanu, M. Tlili, and M. B. Amor, "Synthesis of intermediate crystal Ba1-xCaxSO4 system via co-precipitation of BaSO4-CaSO4 and partial hindrance of gypsum formation," *Desalination and Water Treatment*, vol. 66, pp. 80–87, Mar. 2017, https://doi.org/10.5004/dwt.2017.20188.

[6] J. Moghadasi *et al.*, "Scale Formation in Iranian Oil Reservoir and Production Equipment During Water Injection," in *International Symposium on Oilfield Scale*, Oilfield Scale, UK, Jan. 2003, Art. no. SPE-80406-MS, https://doi.org/10.2118/80406-MS.

[7] E. Bobok, *Fluid Mechanics for Petroleum Engineers*. Elsevier Science, 2012.

[8] M. O. Karkush, M. D. Ahmed, and S. M. A. Al-Ani, "Magnetic Field Influence on The Properties of Water Treated by Reverse Osmosis," *Engineering, Technology & Applied Science Research*, vol. 9, no. 4, pp. 4433–4439, Aug. 2019, https://doi.org/10.48084/etasr.2855.

[9] O. Kivan, M. Yusuf, D. Harbottle, and T. N. Hunter, "Removal of cesium and strontium ions with enhanced solid-liquid separation by combined ion exchange and BaSO4 co-precipitation," *Journal of Water Process Engineering*, vol. 59, Mar. 2024, Art. no. 104934, https://doi.org/10.1016/j.jwpe.2024.104934.

[10] O. Milner and W. M. McNabb, "Determination of sulfur as barium sulfate in the presence of ferric iron," *Analytica Chimica Acta*, vol. 4, pp. 386–388, Feb. 1950, https://doi.org/10.1016/0003-2670(50)80060-0.

[11] S. Suryani, H. Heryanto, R. Rusdaeni, A. N. Fahri, and D. Tahir, "Quantitative analysis of diffraction and infra-red spectra of composite cement/BaSO4/Fe3O4 for determining correlation between attenuation coefficient, structural and optical properties," *Ceramics International*, vol. 46, no. 11, Part B, pp. 18601–18607, Aug. 2020, https://doi.org/10.1016/j.ceramint.2020.04.170.

[12] T. Hussain, V. K. Asfora, B. P. A. G. da Nobrega, V. S. M. de Barros, W. M. de Azevedo, and H. J. Khoury, "Thermoluminescence properties of nanocrystalline BaSO4 doped with Eu2+ produced by solid state combustion synthesis," *Radiation Physics and Chemistry*, vol. 186, p. 109531, Sep. 2021, https://doi.org/10.1016/j.radphyschem.2021.109531.

[13] L. T. MacHale and R. G. Finke, "Solid Barium Sulfate Formation from Aqueous Solution: Re-examination of Key Literature and Kinetics of This Classic System in Search of a Minimum Mechanism of Formation," *Industrial & Engineering Chemistry Research*, vol. 62, no. 25, pp. 9639–9661, Jun. 2023, https://doi.org/10.1021/acs.iecr.3c00875.

[14] A. E. Nielsen, "Electrolyte crystal growth mechanisms," *Journal of Crystal Growth*, vol. 67, no. 2, pp. 289–310, Jul. 1984, https://doi.org/10.1016/0022-0248(84)90189-1.

[15] B. Lo and T. D. Waite, "Structure of Hydrous Ferric Oxide Aggregates," *Journal of Colloid and Interface Science*, vol. 222, no. 1, pp. 83–89, Feb. 2000, https://doi.org/10.1006/jcis.1999.6599.

[16] A. Korchef, "Effect of Iron Ions on the Crystal Growth Kinetics and Microstructure of Calcium Carbonate," *Crystal Growth & Design*, vol. 19, no. 12, pp. 6893–6902, Dec. 2019, https://doi.org/10.1021/acs.cgd.9b00503.

[17] V. Ramaswamy, R. M. Vimalathithan, and V. Ponnusamy, "Synthesis and Characterization of BaSO4 Nano-particles Using Micro-emulsion Technique," *Advances in Applied Science Research*, vol. 1, no. 3, pp. 197–204, 2010.

[18] P. Cambier, "Infrared study of goethites of varying crystallinity and particle size: I. Interpretation of OH and lattice vibration frequencies," *Clay Minerals*, vol. 21, no. 2, pp. 191–200, Jun. 1986, https://doi.org/10.1180/claymin.1986.021.2.08.

[19] Y.-H. Chen, E. Huang, and S.-C. Yu, "High-pressure Raman study on the BaSO4–SrSO4 series," *Solid State Communications*, vol. 149, no. 45, pp. 2050–2052, Dec. 2009, https://doi.org/10.1016/j.ssc.2009.08.023.

[20] E. Melliti, K. Touati, B. Van der Bruggen, and H. Elfil, "Effect of Fe2+ ions on gypsum precipitation during bulk crystallization of reverse osmosis concentrates," *Chemosphere*, vol. 263, Jan. 2021, Art. no. 127866, https://doi.org/10.1016/j.chemosphere.2020.127866.

[21] J. Manam and S. Das, "Characterization and TSL dosimetric properties of Mn doped BaSO4 phosphor prepared by recrystallisation method," *Journal of Alloys and Compounds*, vol. 489, no. 1, pp. 84–90, Jan. 2010, https://doi.org/10.1016/j.jallcom.2009.09.018.

[22] J. Pilátová *et al.*, "Massive Accumulation of Strontium and Barium in Diplonemid Protists," *mBio*, vol. 14, no. 1, Jan. 2023, Art. no. e03279-22, https://doi.org/10.1128/mbio.03279-22.

[23] F. Jones, P. Jones, M. I. Ogden, W. R. Richmond, A. L. Rohl, and M. Saunders, "The interaction of EDTA with barium sulfate," *Journal of Colloid and Interface Science*, vol. 316, no. 2, pp. 553–561, Dec. 2007, https://doi.org/10.1016/j.jcis.2007.09.005.